Chemistry–A European Journal
Research Article
doi.org/10.1002/chem.202303459
Chemistry Europe
European Chemical Societies Publishing
www.chemeurj.org

Design of Multi-Luminescent Silica-Based Nanoparticles for the Detection of Liquid Organic Compounds

Asmira Delic,[a] Mikael Lindgren,[b] Maria Psarrou,[c] Solon Economopoulos,[c] Espen Mariussen,[d, e] Alexander Krivokapic,[f] Ole Torsæter,[g] Mohamed Omran,[g] and Mari-Ann Einarsrud*[a]

Tracer testing in reservoir formations is utilised to determine residual oil saturation as part of optimum hydrocarbon production. Here, we present a novel detection method of liquid organic compounds by monodisperse SiO_2 nanoparticles (NPs) containing two luminophores, a Eu^{III}:EDTA complex and a newly synthesised fluorophore based on the organic boron-dipyrromethene (BODIPY)-moiety. The particles exhibited stable Eu^{III} PL emission intensity with a long lifetime in aqueous dispersion. The fluorescence of the BODIPY was also preserved in the aqueous environment. The ratiometric PL detection technique was demonstrated by using toluene and 1-octanol as model compounds of crude oil. The optimal synthesis conditions were found to give NPs with a diameter of ~100 nm, which is suitable for transport through porous oil reservoir structures. The cytotoxicity of the NPs was confirmed to be very low for human lung cell and fish cell lines. These findings demonstrate the potential of the NPs to replace the hazardous chemicals used to estimate the residual oil saturation. Moreover, the ratiometric PL detection technique is anticipated to be of benefit in other fields, such as biotechnology, medical diagnostics, and environmental monitoring, where a reliable and safe detection of a liquid organic phase is needed.

Introduction

In primary oil recovery, the oil is produced by the pressure difference between the reservoir and the surface.[1] Over time, the oil rate tends to decrease as the reservoir pressure decreases. The secondary recovery aims to stimulate further production through pressure maintenance, i.e., injection of water in nearby areas to push the oil towards the production wells. Even after the secondary recovery, there will normally be substantial amounts of residual oil left in the reservoir. Enhanced oil recovery (EOR) is the tertiary step in which attempts are made to further recover the residual fractions. However, this step is associated with economic risks and demanding oil extraction methods.[2] EOR is believed to be of greater importance to both the increased future energy demand, as well as reducing the environmental impact of oil extraction. The reasons are technical difficulties in discovering and producing from new fields and environmentally sensitive arguments against exploring new fields for oil production.[1,3] Specifically, before starting an EOR operation, it is important to estimate the residual oil saturation in the reservoir to qualify a well in terms of technical feasibility and profitability.

Tracer technology is considered to be the most reliable method to estimate residual oil saturation.[4] Radioactive and non-radioactive chemical tracers,[5] most commonly esters, fluorinated acids, and halogenated benzyl alcohol compounds[6] have been used and proven to be beneficial in gathering reservoir information. The radioactive tracers are no longer applicable in many areas due to regulatory restrictions. There are also increasing environmental concerns about the deployment of chemical tracers due to toxicity and poor biodegradation.[7] Therefore, there is a need for the develop-

[a] Dr. A. Delic, Prof. Dr. M.-A. Einarsrud
Department of Materials Science and Engineering, Trondheim, Norway
Norwegian University of Science and Technology (NTNU)
Sem Sælands vei 12, NO-7491 Trondheim, Norway
E-mail: mari-ann.einarsrud@ntnu.no
[b] Prof. Dr. M. Lindgren
Department of Physics
Norwegian University of Science and Technology
Høgskoleringen 5, NO-7491 Trondheim, Norway
[c] M. Psarrou, Assoc. Prof. Dr. S. Economopoulos
Department of Chemistry
Norwegian University of Science and Technology (NTNU)
Høgskoleringen 5, NO-7491 Trondheim, Norway
[d] Dr. E. Mariussen
Norwegian Institute for Air Research
NO-2007 Kjeller, Norway
[e] Dr. E. Mariussen
Department of air quality and noise
Norwegian Institute of Public Health,
NO-0456 Oslo, Norway
[f] Dr. A. Krivokapic
Institute for Energy Technology
NO-2007 Kjeller, Norway
[g] Prof. Dr. O. Torsæter, M. Omran
Department of Geoscience and Petroleum
Norwegian University of Science and Technology
S. P. Andersens veg 15a, 7031 Trondheim, Norway

Supporting information for this article is available on the WWW under https://doi.org/10.1002/chem.202303459

ment of new environmentally friendly detection methods for the hydrocarbon phase that can replace hazardous chemicals.

Within the fields of biotechnology,[8] medical diagnostics,[9] and environmental reporting,[10] the research activity of luminescence-based detection has been driven by the desire to eliminate radioactive labelling. Luminescence-based analysis has become a standard tool in numerous analytical applications because of the high sensitivity, high temporal resolution, and low-cost testing[11] and could therefore have potential in oil-field applications.[12] The most commonly used luminescent labels are organic dyes and lanthanide(III) complexes.[13] The typical limitations of molecular luminophores, such as poor photostability and aggregation under physiological conditions, have been addressed by the fast and wide research on nanomaterials over the last few decades. Several luminescent compounds with unique optical properties have been developed, such as lanthanide-doped inorganic particles.[14] Also, better control over the synthesis parameters has enabled the development of more complex structures with new luminescence-based detection mechanisms, for example, by merging different luminophores into one nanosized unit.[8b] The advantages of these luminescent nanomaterials have only recently started to be explored for oil-field applications.[15] However, the few reports that exist on luminescent nanomaterials are mainly concerned with the propagation ability of the NPs through the porous reservoir structure, their stability under the targeted conditions, or probing pH and temperature in the reservoirs.[12b,16] Fluorescent nanoparticles for oil sensing applications have recently been reported by Khan et al.[17] There, the focus was to modify the surface chemistry of zinc oxide encapsulated silica NPs to control the dispersibility in the water-containing systems and obtain emission stability under harsh reservoir conditions. Although these nanomaterials have certain promising properties, there is still a lack of proposals for how their luminescence can be used to estimate the remaining oil in the reservoirs.

The aim of this work has been to demonstrate the concept of a novel detection method for liquid organic compounds (LOCs) with luminescent nanoparticles that can be used in oil-field applications, as shown in Figure 1. The idea is partially based on the report of Agenet[12b] describing water tracers, where specific luminophores were incorporated into SiO_2 NPs. In the present work, the detection concept is based on ratiometric luminescence intensity between two luminophores inside a nanoparticle. One of the luminophores acts as a probe towards the LOC, e.g., the reservoir oil, whilst the second acts as the reference. For this concept, several challenges must be solved. First, suitable luminophores that can act as a probe towards the LOCs must be found. Second, a synthesis method has to be developed for the incorporation of the luminophores that yields hydrophilic NPs since water injection is the only way they can be introduced into and recovered from a reservoir. Third, the NPs should have the ability to detect LOCs from an aqueous dispersion. These challenges have been approached by developing an NP particle concept with doubly luminescent silica NPs. A Eu^{III}:EDTA complex and the water-insoluble organic dye based on the boron-dipyrromethene chromophore (BODIPY) were embedded in a silica sphere, as illustrated in Figure 1, by using a modified Stöber method. In addition, the Pluronic® copolymers L-121 and P-123 were also co-incorporated into the

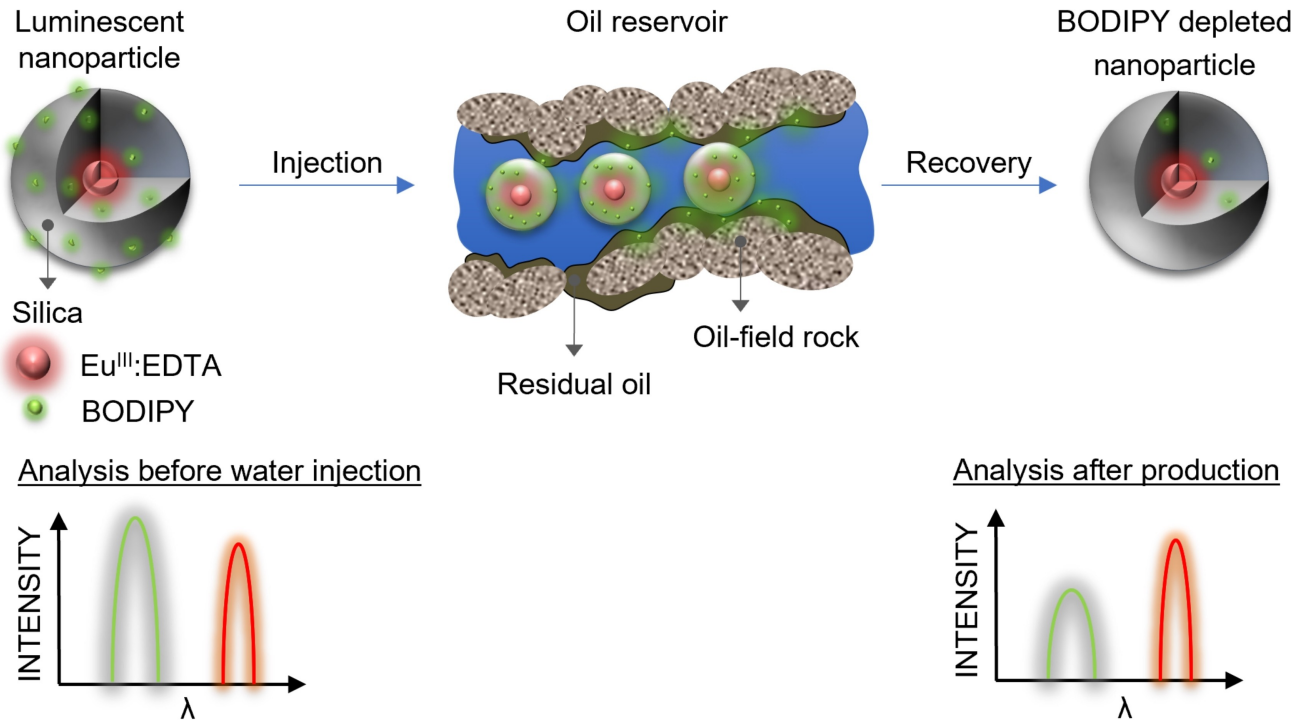

Figure 1. Illustration of the NP concept with two luminophores contained into one unit; silica NP with Eu^{III}:EDTA and BODIPY, and the ratiometric luminescence detection concept. The luminescence intensity of the water-insoluble organic dye BODIPY in the NPs decreases after propagation through the oil-field rock because of the dye release into the residual oil phase.

silica NPs to examine whether their hydrophobic block poly(propylene oxide) (PPO) contributes to higher uptake of BODIPY in the NPs. The ability of the silica NPs to detect LOCs via ratiometric luminescence intensity was probed using toluene and 1-octanol as model compounds of crude oil. In this first proof of the detection concept, applications of these transparent solvents allowed for the omittance of the autofluorescence from crude oil, which otherwise could interfere with the emission from the doubly luminescent SiO_2 NPs. Toluene and 1-octanol also have closer solvent power to crude oil, compared to pure alkanes, such as e.g., isooctane. The toxicity of the NPs and their ability to move through a porous sandstone have been evaluated. It is noted here that we, for simplicity, choose to work with luminescence in the visible range and a transparent model system for the oil/water phases. In industrial applications, the transmission of an oil-containing phase is usually limited in the visible range. The europium and BODIPY can then be replaced by suitable lanthanide and organic dye systems with emission in the infrared region.

Results

Incorporation of Eu^{III}:EDTA into SiO_2 NP

The size and morphology of the Stöber SiO_2-based NPs depend strongly on the precursors, additives, and their concentration.[18] Addition of the Eu^{III}:EDTA complex solution with molar ratios of 1:2, 1:4, and 1:6 into the SiO_2 synthesis resulted in NPs with dark spots in the cores. These spots are marked with the red rings in the TEM images in Figure 2. For all three samples, the average hydrodynamic diameters obtained by DLS measurements were larger than the values obtained from TEM (Table 1). The 1:2 Eu^{III}:EDTA SiO_2 NPs had the largest average particle diameter (149 nm), whilst the 1:4 Eu^{III}:EDTA SiO_2 NPs had the smallest (116 nm).

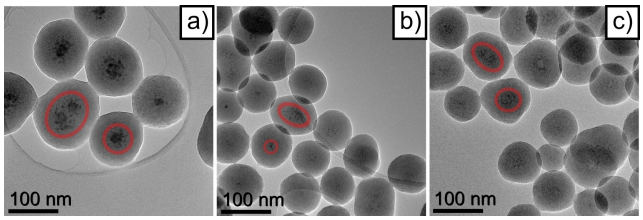

Figure 2. TEM images of the SiO_2 NPs with Eu^{III}:EDTA complex solution of molar ratios: a) 1:2, b) 1:4, and c) 1:6 in the Stöber synthesis. The dark spots in the core of the NPs are Eu^{III}:EDTA complex aggregates[19] (marked with red rings).

Table 1. TEM and DLS derived particle size with polydispersity index (PDI) and zeta potential (ζ) for the SiO_2 NPs with Eu^{III}:EDTA complex solution of molar ratios: 1:2, 1:4, and 1:6 in the Stöber synthesis.

Sample	TEM[a]	DLS[b]		ζ [b,c]
	Avg. d. (nm)	Avg. d. (nm)	PDI	(mV)
1:2	124 ± 19	149 ± 1.2	0.02 ± 0.006	−67 ± 1
1:4	82 ± 14	116 ± 0.2	0.05 ± 0.004	−60 ± 1
1:6	92 ± 10	126 ± 0.9	0.03 ± 0.020	−64 ± 1

[a] Average of 30 particles with standard deviation. [b] The error values represent the standard deviation of a set of triplicate measurements. [c] pH of the aqueous particle dispersion was not adjusted.

FTIR spectra of the 1:4 Eu^{III}:EDTA SiO_2 NPs and the pure SiO_2 NPs are presented in Figure 3 a) and b), respectively. The characteristic silica bands appear between 800 and 1220 cm^{-1} in both spectra.[20] The band at 800 cm^{-1} is assigned to symmetric Si–O–Si stretching. The band at 940 cm^{-1} corresponds to Si-OH stretching.[21] Asymmetric Si–O–Si stretching is evident from the band at 1070 cm^{-1} and the shoulder at 1220 cm^{-1}.[22] The presence of EDTA in the SiO_2 NPs is evident from the bands at 1400 cm^{-1} and 1600 cm^{-1} in spectrum a), which correspond to carboxylate symmetric[23] and asymmetric stretching mode.[20]

PL emission intensity as a function of the Eu^{III}:EDTA molar ratio incorporated into the SiO_2 NPs (1:2, 1:4 and 1:6) was evaluated by integration of their PL emission spectra (Figure 4) in the 570–640 nm range, with the integrals of spectra plotted in the inset. The sample with the highest Eu^{III} amount (1:2 Eu^{III}:EDTA) has the lowest PL intensity. However, it is only ~7% lower than for the 1:6 ratio, which has the highest PL intensity. These results are in line with the report of Elbanowski et al.,[24] who found that the PL intensity of Eu^{III}:EDTA solutions increases with increased excess of EDTA.

Synthesis and incorporation of BODIPY chromophore into the Eu^{III}:EDTA SiO_2; the doubly luminescent nanoparticles

For the design of the organic addend, the BODIPY moiety was chosen as it possesses large extinction coefficients and strong emission characteristics. Although the BODIPY moiety has been one of the most versatile building blocks during the last decades, a simple modification was targeted to afford increased solubility in the chosen solvents and no overlap with the Eu^{III}-based ligand's signals. For this, a new a,b-unsubstituted meso-alkylated BODIPY was chosen where the long alkyl chain was

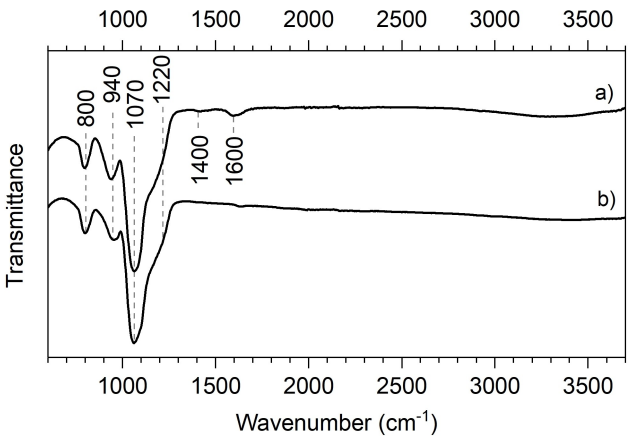

Figure 3. FTIR spectra of a) SiO_2 NPs with 1:4 Eu^{III}:EDTA in the synthesis and

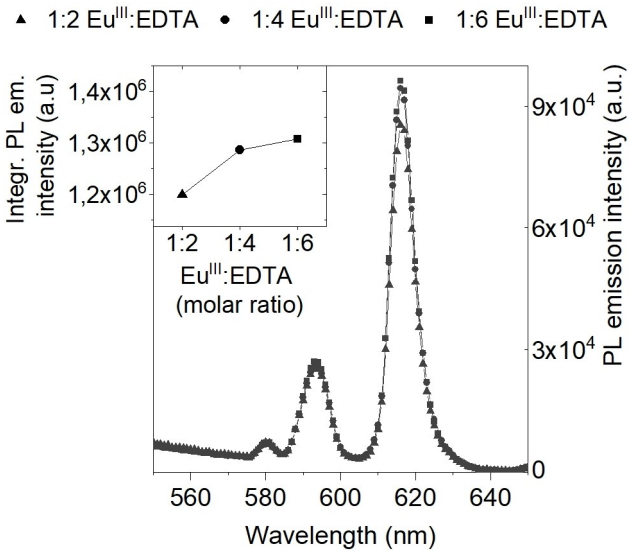

Figure 4. PL emission spectra of SiO_2 NPs aqueous dispersions (0.1 wt%) synthesised with 1:2, 1:4 and 1:6 molar ratios of Eu^{III}:EDTA, at the excitation wavelength of 395 nm. Insert: sum of the integrated PL emission intensities of the bands at 580, 594 and 616 nm for the three samples.

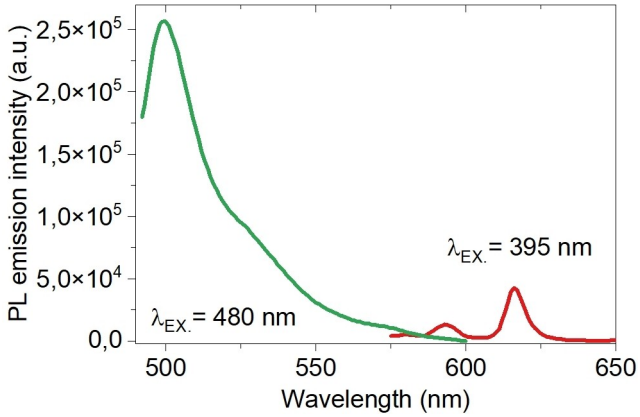

Figure 5. PL emission spectra of an aqueous dispersion of SiO_2 NPs synthesised with 1:4 Eu^{III}:EDTA and BODIPY. Green: BODIPY emission (excitation wavelength 480 nm). Red: Eu^{III} emission (excitation wavelength 395 nm).

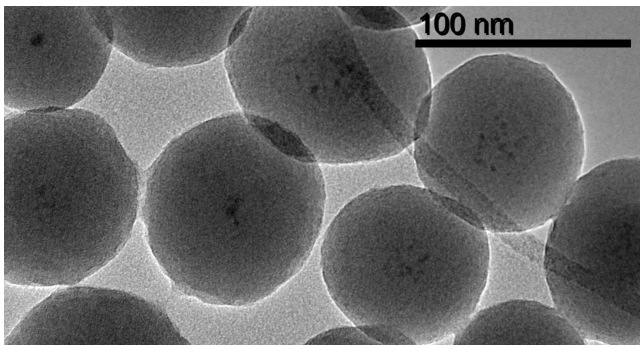

Figure 6. TEM image of the doubly luminescent SiO_2 NPs showing a homogeneous structure with the dark Eu(III) spots in the core.

chosen to facilitate solubility and reduce aggregation phenomena. The synthesis was carried out in a "one-pot" fashion using freshly distilled pyrrole instead of the widely used substituted pyrrolo-analogues. The synthetic scheme and structural characterisation of the chromophore are shown in Figures S10 and S11, respectively.

The NPs synthesised with 1:4 Eu^{III}:EDTA were chosen for further incorporation of the BODIPY dye because this complex ratio gave the smallest particle diameter (Table 1). The incorporation of BODIPY into the NPs was confirmed by the PL emission spectrum seen in green at the excitation wavelength of 480 nm in Figure 5. The spectrum of Eu^{III} emission (red) at the excitation wavelength of 395 nm is also included to demonstrate the doubly luminescent SiO_2 NPs. The TEM image in Figure 6 shows the morphology of these NPs. The BODIPY dye molecules are presumably distributed through the volume of the SiO_2 NPs since the particle structure appears to be homogeneous, apart from the dark Eu(III) core spots.

Optical properties of the doubly luminescent SiO_2 NPs

The differences in the environment of Eu^{III} are probed through a comparison between the excitation and emission spectra of the Eu^{III}:EDTA in the SiO_2 NPs, the Eu^{III}:EDTA aqueous solution, and the Eu^{III}:EDTA dissolved in a mixture of ethanol and NH_3(aq); (NH_3&EtOH), see Figure 7 a-b. The Eu^{III}:EDTA aqueous solution refers to the one prepared for addition into the Stöber synthesis of the SiO_2 NPs. The Eu^{III}:EDTA dissolved in ethanol and NH_3(aq) refers to the one added into the Stöber synthesis before the addition of TEOS, i.e., before the formation of the SiO_2 NPs.

The sharp bands in all excitation and emission spectra are the typical features of Eu^{III}. The bands in the 350–500 nm excitation region (Figure 7a)) correspond to the $^7F_0 \rightarrow {}^5D_4$ (362 nm), $^7F_0 \rightarrow {}^5L_6$ (395 nm), $^7F_1 \rightarrow {}^5D_3$ (416 nm) and $^7F_0 \rightarrow {}^5D_2$ (465 nm) transitions.[25] The emissions of the $^5D_0 \rightarrow {}^7F_{0,1,2,3,4}$ transitions of the Eu^{III} ion (Figure 7 b)) are observed in the 580–700 nm region. The bands of the highest intensity are at 594 nm ($^5D_0 \rightarrow {}^7F_1$), 616 nm ($^5D_0 \rightarrow {}^7F_2$), and 680–710 nm ($^5D_0 \rightarrow {}^7F_4$). The weak intensity bands at 580 and 651 nm correspond to the forbidden $^5D_0 \rightarrow {}^7F_0$ and $^5D_0 \rightarrow {}^7F_3$ transitions,[25a] respectively.

In the excitation spectra, Figure 7 a), a prominent difference in the fine structure is observed, marked with grey areas. In area I, the $^7F_0 \rightarrow {}^5D_4$ (362 nm) band is broad in the spectrum of the SiO_2 NPs, and the Eu^{III}:EDTA in NH_3&EtOH. The corresponding band is rather sharp and consists of two bands in the spectrum of the Eu^{III}:EDTA aqueous solution. Area II marks the 370–390 nm region, where the fine structure is more clearly resolved for the Eu^{III}:EDTA aqueous solution, whilst the Eu^{III}:EDTA in NH_3&EtOH shows band broadening. The spectrum of the SiO_2 NPs resembles both former spectra, with a broad band and a barely visible fine structure. In area III, a weak band at ~490 nm is apparent in the spectrum of the SiO_2 NPs. This emission is a contribution from the BODIPY present in the particles, to be more discussed below.

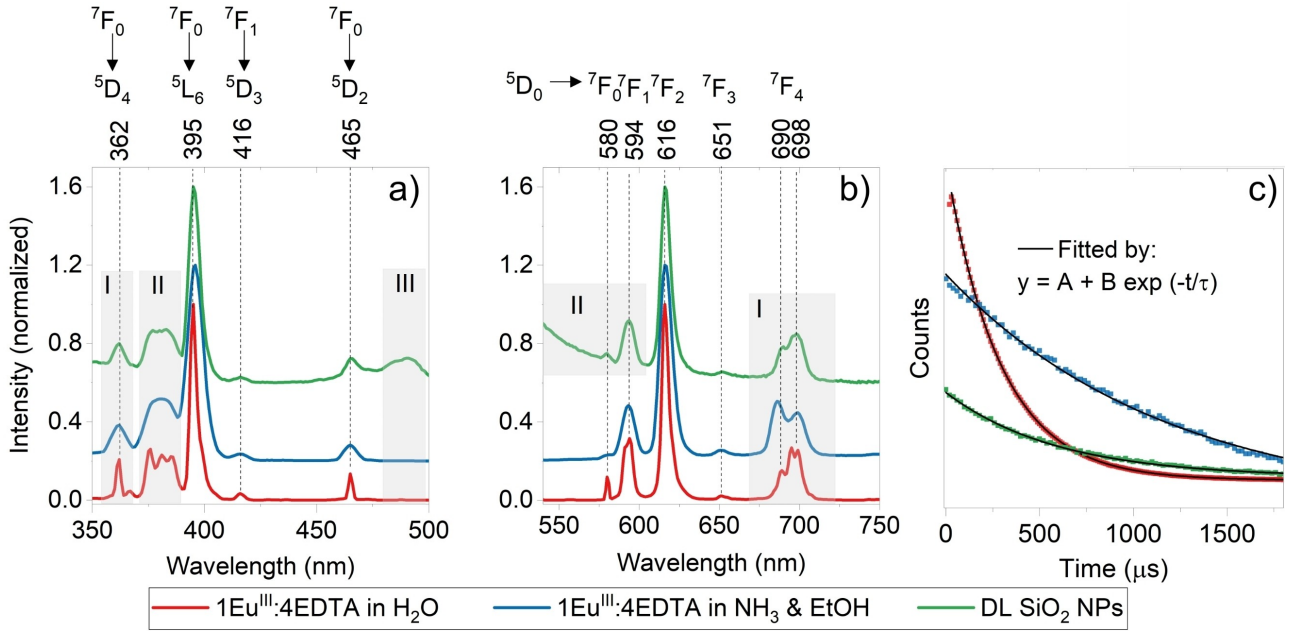

Figure 7. a) Excitation (emission wavelength 616 nm) and b) emission (excitation wavelength 395 nm) spectra of 1Eu^{III}:4EDTA in H_2O, 1Eu^{III}:4EDTA in NH_3&EtOH and 1Eu^{III}:4EDTA in doubly luminescent (DL) SiO_2 NPs in aqueous dispersion (0.1 wt.%). The molar Eu^{III}:EDTA ratio equals 1 : 4 in all samples. The grey areas highlight the differences in spectra described in the text. c) Time-resolved PL decay curves of 1Eu^{III}:4EDTA in H_2O, 1Eu^{III}:4EDTA in NH_3&EtOH and 1Eu^{III}:4EDTA in SiO_2 NPs with an excitation wavelength of 395 nm and emission wavelength 616 nm, fitted with a single-exponential function. The calculated average lifetime ($\tau_{ave.}$) values are given in Table 2.

The emission spectra in Figure 7 b) reveal variations in the fine structure, as marked with the grey area I. The structure of the $^5D_0 \rightarrow {}^7F_4$ (680–710 nm) transition in the spectrum of the SiO_2 NPs is slightly broadened but still resembles the equivalent structure in the spectrum of the Eu^{III}:EDTA aqueous solution. The emission at the 690 nm band of the $^5D_0 \rightarrow {}^7F_4$ transition in the spectrum of Eu^{III}:EDTA in NH_3&EtOH is somewhat larger than the corresponding band in the other two cases. In the spectrum of the SiO_2 NPs, the emission intensity has a slight contribution from the BODIPY emission, marked by the grey area II.

The intensity of the bands in the emission spectra varies with the environment of Eu^{III}. The intensity ratio between the 616 and 594 nm emission bands, defined as $\eta = I(^5D_0 \rightarrow {}^7F_2)/I(^5D_0 \rightarrow {}^7F_1)$ can be used to compare the hydration states of different Eu^{III} compounds.[24,26] The η values were calculated from the ratio of the integrated 616 and 594 nm emission band intensities of the spectra, as shown in Figure S1. Integration ranges were set to 610–630 nm and 585–600 nm for the bands at 616 and 594 nm, respectively. The results are collected in Table 2. The lowest η (2.8) results from the spectrum of Eu^{III}:EDTA complex in water, whilst the spectrum of Eu^{III}:EDTA complex in NH_3&EtOH gives the highest η (3.7). These results are consistent with the previous report on η for Eu^{III}:EDTA as a function of pH. [24] The effect of pH on the Eu^{III} emission is correlated with the acid dissociation constants of EDTA of 1.99, 2.67, 6.16, and 10.26. [27]

At higher pH, such as 11.6 for the 1Eu^{III}:4EDTA complex in ethanol and NH_3(aq) (Table 2), the chelating action of EDTA becomes stronger with the dominating $EDTA^{4-}$ species. At lower pH, such as 5.8 in the Eu^{III}:4EDTA complex in water, the chelating action of EDTA is weaker with the presence of the H_2EDTA^{2-} and $HEDTA^{3-}$ species, which are probably in competition with the Eu^{III} ions' strong preference for water molecules as ligands. Water molecules in the local Eu^{III} environment contribute to nonradiative emission from the excited level through O–H vibrations, which leads to lower η.[24,28] Upon incorporation of the Eu^{III}:EDTA complex into the SiO_2 particles, the basic conditions (pH = 11.6) might have contributed to a lower number of water molecules surrounding the Eu^{III} ion and a higher EDTA chelating ability. Once encapsulated, the SiO_2 acts as a protective layer of the complex against water and can explain the high η (3.4) obtained from the spectrum of the SiO_2 NPs.

Table 2. The intensity ratio between the 616 and 594 nm wavelength emission bands where $\eta = I\ (^5D_0 \rightarrow {}^7F_2)/I\ (^5D_0 \rightarrow {}^7F_1)$ is calculated from spectra in Figure S1. Average lifetime ($\tau_{ave.}$) is obtained from the fitting curves in Figure 7 c) for 1Eu^{III}:4EDTA in H_2O, 1Eu^{III}:4EDTA in NH_3&EtOH, and sample 1Eu(4EDTA) SiO_2 NPs aqueous dispersion. pH values of the solutions are included.

Sample	η	$\tau_{ave.}$ (μs)	pH
1Eu^{III}:4EDTA in H_2O	2.8	289.5 ± 0.3	5.8
1Eu^{III}:4EDTA in NH_3&EtOH	3.7	1172.1 ± 5.2	11.6
DL SiO_2 NPs	3.4	594.6 ± 5.2	7.7

The lifetime of the excited level of Eu^{III} complexes in aqueous solutions is sensitive to the ligand environment and especially the number of water molecules.[28c] Average lifetimes were obtained from PL decay curves of SiO_2 NPs, Eu^{III}:EDTA aqueous solution, and Eu^{III}:EDTA in ethanol and NH_3(aq),

presented in Figure 7 c). Good deconvolution fits of the curves were obtained by using a single-exponential function (solid lines in Figure 7 c). The resulting average lifetime, summarised in Table 2, was the shortest for the Eu^{III}:EDTA aqueous solution at ~290 μs. This value is close to the one obtained by Kropp et al.[28c] for the Eu^{III}:EDTA complex in H_2O (260 μs), but the ratio of Eu^{III} to EDTA was not reported. Incorporation of the complex into SiO_2 doubles the average lifetime to ~595 μs. The longest average lifetime was obtained for the Eu^{III}:EDTA in ethanol and NH_3(aq). These results follow a similar trend as the η values in Table 2.

The absorbance and emission (excitation wavelength 480 nm) spectra of BODIPY in ethanol and the emission spectrum of SiO_2 NPs are shown in Figure S2. Besides a small shift (from 500 to 502 nm) in the maximum of the emission band, the emission spectra of pure BODIPY in ethanol and BODIPY incorporated into SiO_2 NPs are very similar. The small shift is probably due to different solvents,[11] as the SiO_2 particles containing BODIPY were dispersed in water. The SiO_2 matrix and the aqueous environment used as the dispersant of the NPs do not affect the BODIPY emission significantly, which is a tremendous advantage of the dye for the intended application.

Time Correlated Single Photon Counting (TC SPC) decay curves of SiO_2 NPs and BODIPY in ethanol are displayed in Figure S3a) and b), respectively. Contrary to the long lifetime observed for Eu^{III} PL (hundreds of microseconds), the fitted fluorescence lifetime of BODIPY PL was 6.6 ns, demonstrating another major difference between the two luminophores in the present work.

Incorporation of Pluronic® into doubly luminescent silica nanoparticles

The hydrodynamic diameters of particles synthesised with L-121 or P-123 in the concentration range of 12–144 μmol, together with SiO_2 NPs without any Pluronic®, are plotted in Figure S4a). The particles synthesised with L-121 are smaller (110–140 nm) than the particles synthesised with equal molar amounts of P-123. The sample with the lowest L-121 concentration (12 μmol) resulted in particles of smaller diameter (110 nm) compared to the diameter of particles without any Pluronic® (~120 nm). The size range for the particles with P-123 was 140–170 nm. The larger size of these particles compared to the L-121 samples could be due to the higher molar mass percentage of poly(ethylene oxide) in P-123, which expands the resulting SiO_2 particles.

The absolute zeta potential values of the resulting particles (Figure S4b)) decreased upon the addition of L-121 or P-123 to the SiO_2 NPs. None of the aqueous dispersions of the samples was pH adjusted before the zeta potential analysis. The highest absolute zeta potential was obtained for the particles without Pluronic®, with a value of −60 mV, whilst the values for the particles with the Pluronic® were in the −45 to −55 mV range.

Detection of liquid organic compounds; BODIPY release from the doubly luminescent silica nanoparticles

To examine how the release of BODIPY from the SiO_2 NPs into the LOCs varies with time and solvent type, tests were performed for 0.25, 2, 8, 24, and 48 h contact time with toluene or 1-octanol. The PL emission spectra before and after contact with the organic liquids at the given time intervals are shown in Figure 8 a) for release into toluene and b) for release into 1-octanol. The intensity of the band at 480 nm excitation wavelength, i.e., emission from BODIPY in the NPs, decreases with each increasing time interval up to 24 h, where the maximum release is achieved; this is observed with both toluene and 1-octanol. The percentage of BODIPY release from the NPs (eq. 3, Experimental Section) for each time interval is given in Table 3 and plotted in Figure S5. At the shortest time interval (0.25 h), the release is slightly higher in toluene (~7%) than in 1-octanol (~5%). In subsequent time intervals up to 24 h, the same amount of BODIPY is released into the two solvents. For release into toluene, the maximum is reached at the 24 h time interval with ~60%, and no further increase is observed. For 1-octanol, the maximum amount of BODIPY released from the NPs was ~64% after 48 h contact time. The quantitative results take into account the decrease in the Eu^{III} emission using eq. (2). This decrease, i.e., the spectra at 395 nm excitation wavelength, is significant after contact with the LOCs, as is apparent from Figure 8 a-2) and b-2). The calculated intensity decrease is listed in Table 3 for each time interval. At the longest contact time (48 h), the intensity of Eu^{III} emission drops by 27% and 21% after contact with toluene and 1-octanol, respectively.

Table 3. Percentage BODIPY release in toluene and 1-octanol for doubly luminescent SiO_2 NPs at different contact time intervals. The release was calculated by eq. (3) (see Experimental Section) as an average of the three parallels for each time interval. The percentage decrease in intensity of integrated Eu^{III} PL emission spectra at excitation wavelength 395 nm, before and after contact with toluene and 1-octanol for different time intervals, calculated using eq. (4) (see Experimental Section). The error values represent the standard deviation of a set of triplicate measurements.

Time interval [h]	BODIPY release from the NPs in:		Decrease in Eu^{III} PL emission intensity in:	
	Toluene [%]	1-Octanol [%]	Toluene [%]	1-Octanol [%]
0.25	7.3 ± 1.6	5.2 ± 0.6	1.3 ± 0.7	0.7 ± 0.5
2	19.4 ± 0.2	19.6 ± 1.2	7.5 ± 0.8	5.6 ± 1.5
8	40.3 ± 0.8	39.6 ± 0.2	13.3 ± 0.9	7.5 ± 1.1
24	60.0 ± 0.4	60.6 ± 0.4	26.7 ± 2.8	26.3 ± 0.7
48	60.9 ± 0.6	64.3 ± 0.7	27.0 ± 7.2	21.2 ± 1.9

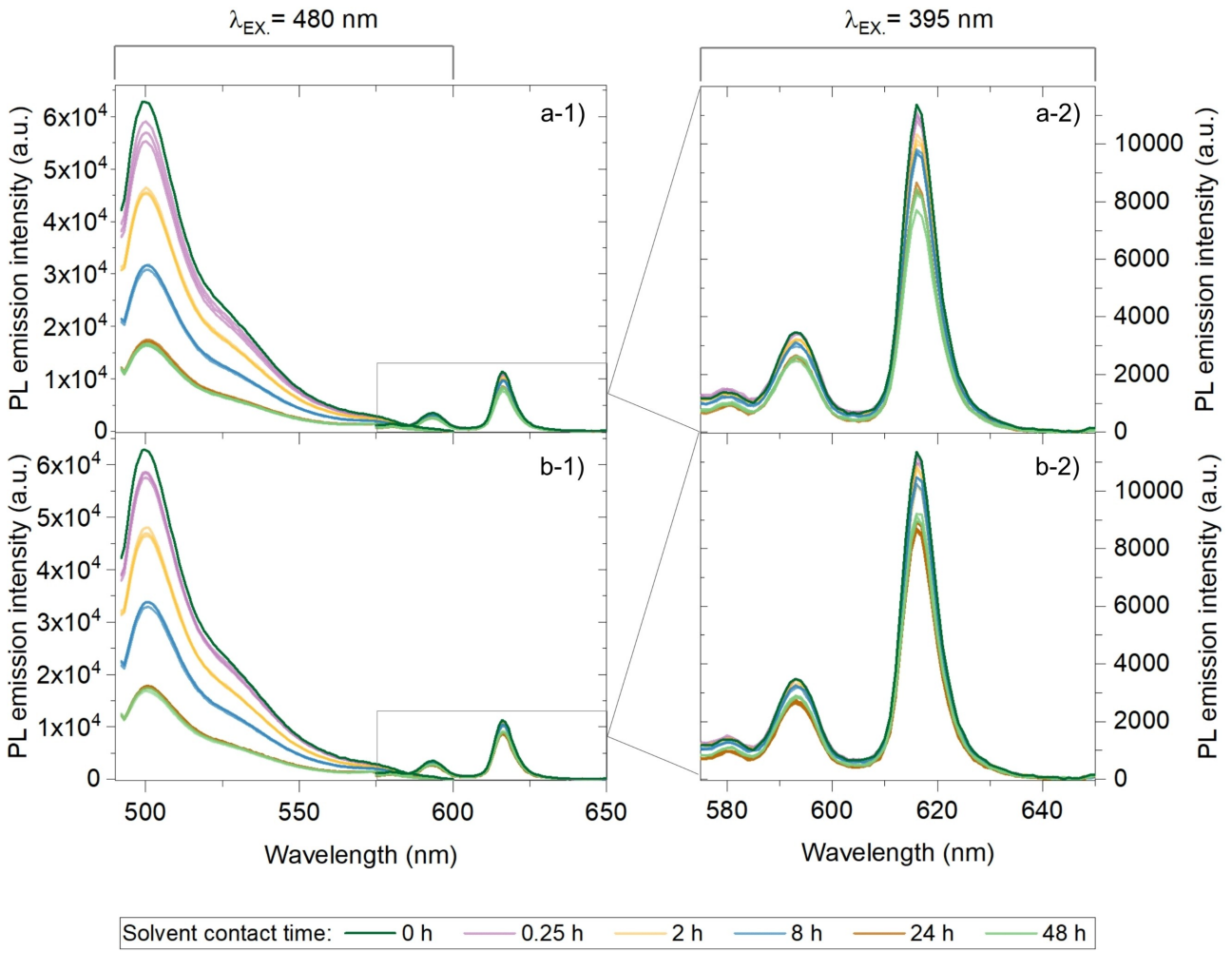

Figure 8. PL emission spectra of doubly luminescent SiO_2 NPs aqueous dispersion (0.1 wt.%) at excitation wavelength 480 nm and 395 nm before and after contact with a) toluene and b) 1-octanol for 0, 0.25, 2, 8, 24 and 48 h. The dark green spectra are of the aqueous dispersion of the NPs before contact with the LOCs. The spectra in all other colours are of the aqueous dispersion after contact with toluene at given time intervals, each run in three parallels (A, B, C). a-2) and b-2) Magnified spectra from a-1) and b-1), respectively, at excitation wavelengt 395 nm.

The dye release testing was also performed for the samples with Pluronic®. The samples with the smallest particle diameters were chosen for the tests, i.e., 18P, 18 L, 24 L, 36 L, 72 L, and are compared to the doubly luminescent SiO_2 NPs without Pluronic®. Figure S6 shows the PL emission spectra of aqueous dispersions of the samples before and after contact with toluene for 24 h. A significant intensity decrease is seen in the spectra of BODIPY emission (480 nm excitation wavelength) for all samples after contact with toluene. The calculated percentage corrected BODIPY release as a function of the Pluronic® concentration in the doubly luminescent SiO_2 NPs is given in Table S1 and plotted in Figure S7. Particles synthesised without any Pluronic® had ~52% of BODIPY released into toluene. The sample with P-123, i.e., 18P, had the lowest amount of BODIPY released (~33%). The particles with L-121 showed a progressive increase in the BODIPY release with increasing L-121 concentration, with ~35% for 18 L and the highest value of ~58% for 72 L. The small standard deviation calculated for each sample in Figure S7 confirms the reproducibility and the precise response of the BODIPY release from the SiO_2 NPs particles into toluene.

Toxicity test

The doubly luminescent particles synthesised with L-121 (36 μmol) and P-123 samples (36 μmol) were tested for their cytotoxic potential with the colony forming efficiency (CFE) assay. The human lung cell line, A549, was exposed for 11 days with a low cell density. No significant effects were observed, even at concentrations as high as 380 μg/mL (Figure 9), indicating a very low cytotoxic potential for both samples.

The doubly luminescent particles synthesised with L-121 (36 μmol) were further evaluated with the comet assay, which was applied to the human lung cell line A549. Concomitant with the comet assay, it is standard to evaluate the cytotoxicity of the test concentrations. The alamarBlue cytotoxicity assay confirmed that the material had no effect on the cell viability (Figure S8 a)). The cytotoxicity of the material was also tested on two fish cell lines to confirm that the effect of the material did not deviate much from the effect on the human lung cell. As shown in Figure S8 b), the sample had no effect on the cell viability of the two fish cell lines, RTgill-w1 and RTH-149, which

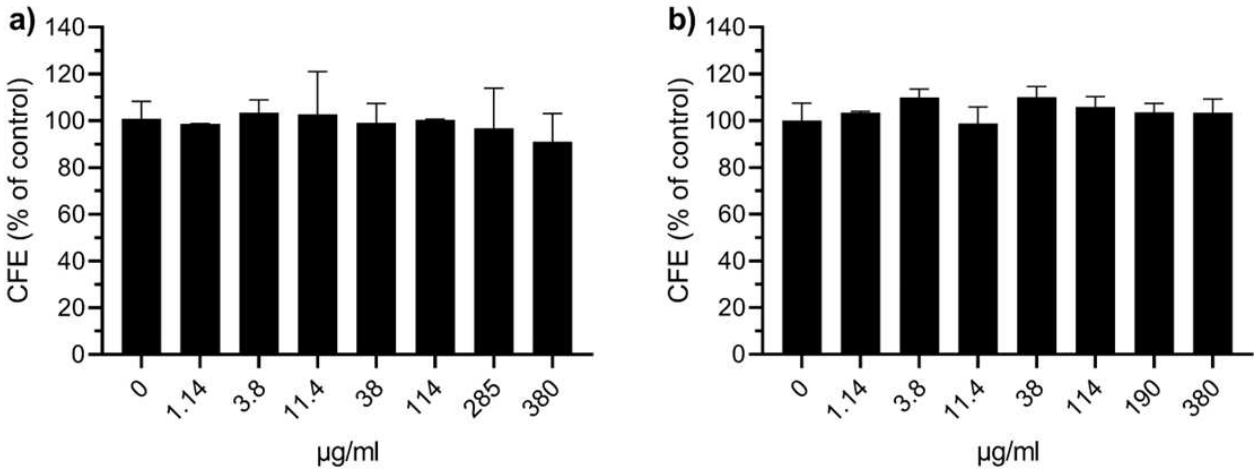

Figure 9. The effect of a) doubly luminescent particles synthesised with L-121 (36 µmol) and b) P-123 samples (36 µmol) on cell viability measured by CFE after submerged exposure of A549 cells. The results are shown as mean ± standard deviation from three (L-121) or two (P-123) independent experiments performed in six replica wells. The cell viability is presented as relative to negative control (non-exposed cells).

are a gill cell line and liver cell line from Rainbow trout, respectively.

The comet assay was applied to indicate the genotoxic effect of the doubly luminescent particles synthesised with L-121 (36 µmol). The particles did not show any effects on the comet assay up to a concentration of 160 µg/mL, nor did it show any increase in genotoxic effects due to the induction of oxidative stress (Figure S9).

Transport testing of silica nanoparticles through sandstone

To test the propagation capability of the doubly luminescent SiO_2 NPs through porous sandstone, the SiO_2 NPs synthesised with $1Eu^{III}$:4EDTA and 0.6 µmol BODIPY, were passed through a natural rock common in oil reservoirs, i.e., a Berea sandstone core.[29] The particles were injected at a concentration of 0.1 wt % in an aqueous dispersion containing 1 wt% NaCl to mimic the low salinity conditions that can be applied in the studies of enhanced oil recovery.[29b,30] Figure 10 shows the measured relative concentration by absorbance and PL of the particles before the injection (normalised to 1) and in the effluent pore volumes.

The minimum C/C_0 of the particles found to pass through the sandstone as measured by absorbance at 400 nm was ~0.8, and the minimum C/C_0 as measured by PL at 480 nm excitation wavelength was ~0.7. The higher concentrations measured by absorbance could be due to the agglomeration of the NPs during the flow through the sandstone. The retention of some particles and blocking of sandstone pores are reflected in the differential pressure curve included in Figure 10. The maximum differential pressure and the minimum C/C_0 of the particles in the effluent were measured for pore volume number 6, as marked by a vertical dotted line in the figure.

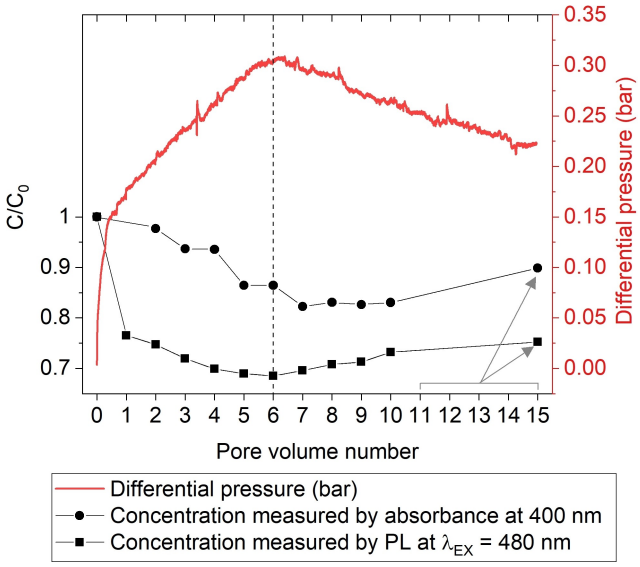

Figure 10. The concentration of doubly luminescent SiO_2 NPs aqueous dispersion in 1 wt% NaCl solution measured before the transport test and for each pore volume injected through a Berea sandstone core. Differential pressure measured over the inlet and outlet of the core is plotted as a function of the injected pore volumes. The maximum differential pressure and the minimum C/C_0 of the particles in the effluent were measured for pore volume number 6, as marked by a vertical dotted line in the figure.

Discussion

The mechanism used to detect the doubly luminescent SiO_2 NPs is based on the release of the BODIPY into the LOCs. Hence, the dye should not be strongly attached to the silica structure. On the other hand, the Eu^{III}:EDTA needs to be protected from any external influence since the PL emission used as the reference signal must be stable. These requirements were met in the sol-gel process by using the one-pot modified Stöber method, which enabled the preparation of monodisperse silica NPs down to 100 nm in diameter with simultaneous incorpo-

ration of the water-insoluble organic dye BODIPY and the Eu^{III}:EDTA complex.

The dark spots observed in the cores of the particles in the TEM images are believed to be molecular aggregates of the Eu^{III}:EDTA precipitate and not the alternative $Eu(OH)_3$ precipitate. In the $Eu(OH)_3$, nonradiative deactivation of the $^5D_0$ level takes place through weak vibronic coupling with the vibrational states of the O–H oscillators,[27] while PL measurements from the SiO_2 NPs clearly displayed Eu^{III} emission (Figure 4). The long PL lifetime (~0.6 ms) also confirms the presence of the Eu^{III}:EDTA in the NPs.[28c] In addition, the presence of EDTA in the SiO_2 was evident from the FTIR spectra (Figure 3).

The silica matrix shielded the Eu^{III} complex in its core, evident from the η value, calculated from the intensity ratio between the 616 and 594 nm emission bands, which was significantly higher for the Eu^{III}:EDTA in the SiO_2 NPs than in H_2O. This implies less nonradiative energy transfer from the excited Eu^{III} ions in the SiO_2 NPs compared to Eu^{III}:EDTA in H_2O.[24,28c] These results suggest that the molecular conformation of the incorporated Eu^{III}:EDTA complex was conserved without direct interaction between the Eu^{III} ions and the O–H groups inside the Si–O–Si network, which would otherwise cause quenching of the Eu^{III} luminescence.[31] Therefore, no annealing was needed to remove the O–H groups and enhance the PL, which is often applied to rare-earth doping of silica.[31–32]

Since no high-temperature treatment was needed, the simultaneous incorporation of the organic dye into the SiO_2 NPs could be conducted. In the first report of the so-called organosilica spheres by Van Blaaderen et al.[33] and in most subsequent reports, the fluorescent dye is modified by chemical bonding to an organofunctional silane, most commonly APTES, before the hydrolysis condensation step.[34] The resulting covalent bonding of the alkoxysilane coupled dye molecules to the polysiloxane network is reported for fluorescein and rhodamine to shift their maximum emission wavelength up to 17 nm compared to free dyes due to the change in the molecular environment.[8a,33] BODIPY incorporated into the SiO_2 NPs in the present work is assumed to be weakly bonded to the silica matrix for several reasons. The chemical structure of the dye (Figure S10) does not contain any functional groups that would promote covalent interaction with the SiO_2 structure. The emission band maximum for BODIPY in the SiO_2 NPs was observed to redshift by only 2 nm compared with the free BODIPY in ethanol. The small shift can be attributed to the difference in polarity of the ethanol and silica matrix/H_2O rather than covalent bonding.[35] The release of BODIPY from the NPs into the LOCs supports a non-covalent assembly.[36]

The removal of the dye from the doubly luminescent SiO_2 NPs upon contact with the LOCs, regarded as a nuisance in many biomedical applications,[36] was in this work used as an advantageous detection technique. The ratiometric detection method was demonstrated by the dye's transport from the NPs in the aqueous phase into the organic phase. The Eu^{III} in the core of the NPs was not affected by the changing environment, reflected in the nearly constant emission intensity. The modulated intensity ratio of the two emissions induced by contact with toluene or 1-octanol permitted the quantitative determination of the BODIPY response.

The BODIPY release from the model systems used here deviates from realistic conditions, in which the flow of the NP aqueous phase through sandstone would sweep over a stationary oil phase. However, to examine the dye release process only, the tests needed to exclude any side effects, such as interactions between the NPs and the sandstone. The amount of BODIPY released in toluene and 1-octanol was shown to be highly predictable by the reproducible behaviour, meaning that the NPs have a reliable response to the targeted analytes. Since toluene and 1-octanol have different polarities (0.099 and 0.528, respectively[35c]), the observation that the release kinetics display similar characteristics in both solvents indicates that the process of BODIPY release is governed by the silica NPs' encapsulation of the dye, i.e., mostly mechanically promoted desorption. This implies that the dye release could potentially be controlled by engineering the adsorption strength to the silica matrix. Molecular engineering of the dye molecule, in particular, should easily fine-tune this property. Thereby, the ability to release dye gradually could be correlated with the amount of residual oil in reservoirs.

The dye release into toluene was slightly higher for the NPs with the highest L-121 concentrations (Figure S7 and Table S1). These tests demonstrate that the copolymer enhances the transfer of the dye from the NP to the organic phase. On the other hand, the resulting particle size was observed to increase when Pluronics® was included in the synthesis. A large expansion in the particle size is not desirable for transport through the small pores of a reservoir structure. Therefore, the optimal L-121 concentration in the synthesis is evaluated to be between 24 and 36 μmol. The transport test did show the ability of the NPs without Pluronics® to propagate through the Berea sandstone, where the minimum C/C_0 of the particles found to pass through the sandstone was ~0.7. The number could potentially be increased by further surface modification of the SiO_2 NPs.[37]

The cytotoxic potential of the doubly luminescent particles synthesised with L-121 and P-123 (36 μmol) was found to be very low for the human lung cell line when tested with the CFE assay, regarded as a sensitive cytotoxicity assay. No significant effects were observed, even at concentrations as high as 380 μg/mL. Also, no genotoxic effects of the NPs due to the induction of oxidative stress were found in the comet assay (Figure S9). Previous studies on the toxicity of amorphous silica particles are inconsistent.[38] The toxicity appears highly dependent on the physico-chemical properties of the particles, such as size and surface chemistry, which is determined by the method of synthesis.[39] The low toxicity of the particles in this study may be because of a preventive effect of Pluronic® in the samples.[40] Agglomeration of the particles on the surface of the cells might have occurred since the culture medium contains various salts, nutrients, and proteins from fetal bovine serum, which are essential for the cultivation of most cell lines. Agglomeration reduces the particle surface area, which is in contact with the cells and may, therefore, reduce their toxicity. The high content of proteins in the culture medium may also

adsorb to the particle surface, forming a protein corona, which may be followed by reduced surface reactivity and toxicity.

The concept developed in this work is the first step towards practical applications of a luminescent-based method for oil detection in reservoirs. The detection principle differs slightly from the classical partitioning interwell tracer test, involving chromatographical separation. Future research should focus on testing the detection method using ratiometric luminescence in sandstones with crude oil to establish a quantitative relationship between the BODIPY departure and residual oil saturation.

Conclusions

The proposed concept of a ratiometric luminescence detector of liquid organic compounds has been confirmed. Monodisperse, ~100-nm-sized SiO_2 NPs with dual luminescence were obtained. The NPs were stable towards agglomeration in an aqueous dispersion due to the electrostatic repulsion reflected in their large negative zeta potential. A stable reference signal was obtained through the Eu^{III} PL emission intensity because the molecular conformation of the complex inside the SiO_2 NPs was preserved to a large extent, which also contributed to a long PL lifetime (~0.6 ms). The physical encapsulation of the dye BODIPY in the NPs allowed its release upon contact with LOCs, serving as probe molecules through their concentration change in the NPs. The time-dependent release of the dye, with a maximum loss of ~60% after 24 h contact time demonstrated the potential of the NPs to function as a detector of an organic phase based on the ratiometric luminescence concept.

Experimental Section

Synthesis of bare SiO_2 nanoparticles

SiO_2 NP synthesis was based on the Stöber method.[41] The correlation between the reagent concentrations and the resulting particle size, developed by Bogush et al.[18] was used as the basis for the synthesis. Ethanol (50 mL, VWR Chemicals, 99.97%) and ammonia solution (2.5 mL, Merck, EMSURE® for analysis) were mixed in a 100 mL round bottom flask (pH = 12.15) and heated to 60 °C in a water bath. Tetraethyl orthosilicate (TEOS) (0.8 mL, Sigma-Aldrich, ≥ 99.0%) was added dropwise under magnetic stirring (300 rpm) for the 2 h reaction time. The product was separated from the reaction medium by centrifugation (7500 rpm, 30 min) and washed with Milli-Q® water (80 mL) three times.

Incorporation of Eu^{III}:EDTA complex into SiO_2 nanoparticles

Solutions of the Eu^{III}:EDTA complex were prepared in the following manner: First, a stock solution of 0.115 M EDTA was prepared by mixing EDTA (VWR Chemicals, ≥ 98.0%) with Milli-Q® water. NaOH pellets (Merck, EMSURE® for analysis) were added until the EDTA was dissolved and the solution turned clear (pH = 7). Thereafter, the solution was mixed with $EuCl_3 \cdot 6H_2O$ (Sigma-Aldrich, 99.9%) in different Eu^{III}:EDTA ratios. The complex solution was added before TEOS in the synthesis procedure of SiO_2 NPs, as previously described. An overview of the samples, $EuCl_3 \cdot 6H_2O$ and EDTA amounts, and their molar ratio for each sample's synthesis is given in Table 4.

Synthesis of BODIPY

All the chemicals were purchased from Merck Sigma-Aldrich and were used without further purification unless otherwise stated. In a carefully dried and degassed vial, under nitrogen atmosphere, freshly distilled pyrrole (5.0 mL), palmitoyl chloride (10.0 mL), N,N-diisopropylethylamine (10 mL) along with dichloromethane (120 mL) were added. The mixture

was cooled at −18 °C (ice/acetone bath) and boron trifluoride diethyl etherate (14 mL) was added dropwise. The reaction mixture was left stirring in the bath for 23 h and was allowed to reach room temperature naturally. The reaction mixture was washed with aqueous sodium hydroxide solution (0.1 M, 4×200 mL) and filtered. The organic layer was washed with distilled water (2×200 mL), dried over anhydrous magnesium sulphate, filtered, and concentrated under reduced pressure. The crude product (9.60 g) was filtered through silica gel (ethyl acetate/n-pentane, 1:5 v/v) and evaporated under reduced pressure. The product was purified by column chromatography on silica gel (gradient ethyl acetate/n-pentane, 1:100 to 1:25, v/v). A red solid with a green metallic tint was obtained with a yield of 10% (1.28 g, 3.2 mmol). ^{1}H NMR (400 MHz, $CDCl_3$, δ ppm): 7.84 (s, 2 CH), 7.27 (d, 2 CH, J = 4.2), 6.55–6.51 (m, 2 CH), 2.92 (t, CH_2, J = 8.0), 1.78 (qui, CH_2, J = 7.7), 1.49–1.39 (m, CH_2), 1.39–1.17 (m, 12 CH_2), 0.88 (t, CH_3, J = 6.7) ^{13}C-NMR (400 MHz, $CDCl_3$, δ ppm): 151.3 (C), 143.3 (2 CH), 135.2 (2 C), 127.8 (2 CH), 117.9 (2 CH), 33.9 (CH_2), 31.9 (CH_2), 31.2 (CH_2), 30.1 (CH_2), 29.7–29.6 (6CH_2) 29.4-29.3 (3 CH_2), 22.7 (CH_2), 14.1 (CH_3) R*f* (1:5 ethyl acetate/*n*-pentane): 0.77.

Incorporation of BODIPY into the Eu^{III}:EDTA complex into SiO_2 nanoparticles

The BODIPY (24 mg) was dissolved in ethanol (50 ml). The remaining steps are the same as described in the experimental section on the incorporation of Eu^{III}:EDTA complex into SiO_2 nanoparticles.

Addition of Pluronic® into the synthesis of SiO_2 nanoparticles with Eu^{III}:EDTA

The Pluronic® (Sigma-Aldrich, quality level according to Sigma-Aldrich), either L-121 or P-123, was added to ethanol and sonicated until dissolved (5 min at 37 kHz, Elmasonic P60H, Elma Schmidbauer GmbH, Singen, Germany). The remaining stages of the synthesis were described in the experimental section on the incorporation of Eu^{III}:EDTA complex into SiO_2 nanoparticles. The amounts of Pluronic® added are listed in Table S2. In the sample nomenclature, the letter L or P indicates the Pluronic® type (L-121 or P-123), whilst the digit in front of the letter indicates the copolymer amount in μmol.

Table 4. The synthesis parameters for the preparation of SiO_2 NPs: the amount of solvent and reactants, reaction temperature, and duration.

Sample	EDTA 0.115 M(aq) [mL]	$EuCl_3 \cdot 6H_2O$ [mg]	Molar ratio
1:6 Eu:EDTA SiO_2 NPs	0.34	2.37	1:6
1:4 Eu:EDTA SiO_2 NPs	0.34	3.54	1:4
1:2 Eu:EDTA SiO_2 NPs	0.34	8.26	1:2

Characterisation

Transmission electron microscopy (TEM) imaging was performed using a JEM-2100 200 kV electron microscope (Jeol, Tokyo, Japan). The TEM images were processed with a DigitalMicrograph (Gatan Inc. version 3.32). A Helios G4 DualBeam™ (Thermo Scientific™, Hillsboro, Oregon, USA) was used to cut the particles with a focused ion beam (FIB) and to record scanning electron microscopy (SEM) images. The TEM samples were prepared by deposition of the aqueous dispersions of the particles onto holey carbon film on Cu grids (Lacey, Electron Microscopy Sciences, Hatfield, Pennsylvania, USA). After deposition, the grids were left to dry at ambient temperature for 1 h. The size of the particles was obtained from the TEM images by measuring the diameter of the particles with the image processing program ImageJ. The diameter values reported are the average of the measurements of a certain number of particles, specified in the results, with standard deviation (SD.

A Zetasizer Nano ZS instrument (Malvern Panalytical Ltd, Malvern, UK) and the manufacturer's Zetasizer software were used to obtain the hydrodynamic particle diameter and polydispersity index (PDI) by dynamic light scattering (DLS) in three parallel measurements. The same instrument and software were used to obtain the zeta potential. The hydrodynamic diameter, PDI, and zeta potential of the particles were calculated using the standard settings of the instrument software. The distribution represents the fraction of scattering intensity originating from particles in the respective size class. DLS was used herein as a routine characterisation tool; due to the involved averaging and weighting in DLS, no further attempts to analyse details of the size distribution have been made. When the samples were suspended in Milli-Q® water, the pH was not adjusted before measurements. All measurements were conducted on dispersions with a maximum particle concentration of 0.2 wt%, using a folded capillary zeta cell (DTS1070, Malvern Panalytical Ltd, Malvern, UK). The reported zeta potential and hydrodynamic particle diameter values are the averages of the triplicate measurements and their standard deviation (SD).

Steady-state and μs – ms lifetime photoluminescence measurements were carried out using a PTI Quantamaster 8075–22 (Horiba Scientific, Kyoto, Japan) equipped with Double Mono 300 spectrometer chambers for both excitation and emission. The OB-75X (75 W Xenon arc lamp) was used as the light source for continuous-wave measurements. The QM-400 Phos was used as the light source in time-resolved PL decay measurements of samples with Eu^{III}. A Hamamatsu R928 PMT (Hamamatsu, Japan) was used for detection in the range 185–950 nm. Data acquisition and basic data handling were carried out using the Felix Data Analysis software. UV-transparent cuvettes (Brand) with a 10 mm light path were used for samples dispersed in Milli-Q® water. Quartz cuvettes were used for PL measurements of samples with toluene or 1-octanol. The PL emission spectra were integrated to quantify the amount of BODIPY released. Limits for spectra with excitation wavelengths of 395 nm and 480 nm were set to 575–650 nm and 490–600 nm, respectively. The resulting integrals were defined as follows: $C_{1(Eu)}$ = integral of spectra at 395 nm excitation wavelength *before* contact with LOCs; $C_{2(Eu)}$ = integral of spectra at 395 nm excitation wavelength *after* contact with LOCs; $C_{1(BDP)}$ = integral of spectra at 480 nm excitation wavelength *before* contact with LOCs; and $C_{2(BDP)}$ = integral of spectra at 480 nm excitation wavelength *after* contact with LOCs. The percentage reduction in the emission of the BODIPY before and after contact with LOCs, ΔBDP, is given by:

$$\Delta BDP = [(C_{1(BDP)} - C_{2(BDP)})/C_{1(BDP)}] \cdot 100\,\% \quad (1)$$

Since the emission of the Eu^{III} is used as an internal standard, the BODIPY emission must be corrected by the change in the intensity of the spectra at 395 nm excitation wavelength before and after contact with the LOCs. One way of correcting is to replace $C_{1(BDP)}$ with $C_{1(BDP)}$*, which takes into account the change in the Eu^{III} emission:

$$C_{1(BDP)}{}^{*} = C_{1(BDP)} \cdot (C_{2(Eu)}/C_{1(Eu)}) \quad (2)$$

The percentage corrected BODIPY release, ΔBDP*, is obtained by replacing $C_{1(BDP)}$ with $C_{1(BDP)}$* in eq. (1):

$$\Delta BDP^{*} = [1 - (C_{2(BDP)} \cdot C_{1(Eu)}) / (C_{1(BDP)} \cdot C_{2(Eu)})] \cdot 100\,\% \quad (3)$$

The percentage reduction in the emission of the Eu^{III} before and after contact with LOCs, ΔEu^{III}, is given by:

$$\Delta Eu^{III} = [(C_{1(Eu)} - C_{2(Eu)}) / C_{1(Eu)}] \cdot 100\,\% \quad (4)$$

For each sample, the BODIPY release test was performed in three parallels. The ΔBDP* and ΔEu^{III} were calculated from spectra as an average of the three parallels.

Time-resolved fluorescence measurements of samples with BODIPY were recorded with an IBH time-correlated single-photon counting (TC SPC) system using deconvolution to fit the decays. A laser diode operating at 469 nm (for samples with BODIPY) or 373 nm (for samples with CDs) was used as the excitation source, and the emission was recorded at 500 nm. Measurements were conducted on samples dispersed in Milli-Q® water or ethanol contained in quartz cuvettes. Details of the setup and procedures were previously reported by Glimsdal et al.[42]

Ultraviolet-visible (UV-Vis) spectra were recorded with an Evolution 220 UV-Visible spectrophotometer (Thermo Fisher Scientific, Waltham, Massachusetts, US) equipped with a xenon flash lamp and a dual silicon photodiode detector. The aqueous sample dispersions were contained in UV-Vis transparent cuvettes (UVette® 220–1600 nm, Eppendorf AG, Hamburg, Germany). The step size was set to 1 nm with an integration time of 0.1 s.

Fourier-transform infrared (FTIR) spectra were recorded using a VERTEX 80v vacuum spectrometer (Bruker Optics, Ettlingen, Germany), equipped with a Platinum ATR diamond sampling accessory. For each FTIR spectrum, 128 scans with a resolution of 4 cm^{-1} were acquired. The samples were either dried powders or aqueous dispersions, as specified in the reported results.

^{1}H and ^{13}C NMR spectra were recorded in $CDCl_3$, using the Bruker DPX 400 MHz Avance III HD NMR spectrometer (Figure S11).

Testing of BODIPY release from the doubly luminescent SiO_2 NPs

Aqueous dispersions of the NPs were prepared by suspending a ~0.1 wt% sample in Milli-Q® water (15 mL), and steady-state PL measurements were performed for the dispersion. The dispersion was divided into three equal volumes (i.e., three parallels). Toluene (5 mL, Sigma-Aldrich, ≥ 99.5 %) or 1-octanol (5 mL, Sigma-Aldrich, ≥ 99.0 %) was added to each aqueous dispersion volume in a glass vial. The vials were then placed on a rotator (45 rpm) for 0.25, 2, 8, 24, or 48 h to induce contact between the aqueous and the organic phases. These time intervals are referred to as contact time with the organic phase in the results sections. After spontaneous separation of the phases, 3 mL of the aqueous phase at the bottom of the glass vial was withdrawn with a needle (16G, L 1.5 in, Precisionglide, B–D, New Jersey, US) and syringe (SOFT-JECT® 5 mL, Henke-Sass Wolf, Tuttlingen, Germany), to avoid any collection of the organic phase. Finally, steady-state PL was measured for the aqueous phase and the organic phase.

Toxicity testing

The toxicity methodology is described in Supporting Information.

Transport testing through sandstone

The doubly luminescent SiO_2 NPs (1.0 g) were dispersed in Milli-Q® water (1 L) containing sodium chloride (10 g, Sigma-Aldrich, ≥ 99.5 %). Steady-state PL and UV-Vis measurements were recorded for the dispersion before and after transport through a Berea sandstone. The experimental setup and details about the experiments for the transport testing are further described in Supporting Information.

Supporting Information

The authors have cited additional references within the Supporting Information.

Acknowledgements

Prof. Dr. M–A. Einarsrud, Dr. A. Krivokapic, and Dr. A. Delic designed the study. Dr. A. Delic has conducted all the experimental work except for the following: The synthesis of the BODIPY dye was performed by Maria Psarrou and Assoc. Prof. Solon Economopoulos. The time-resolved PL decay measurements and the fitting of the decays in Figures 7 c) and S3 were performed by Prof. Dr. Mikael Lindgren, who also contributed to all PL data collection and analysis. Most of the toxicity tests were performed by senior scientist Dr. E. Mariussen. Work was, in addition, performed by senior scientists E. Longhin, N. El Yamani, and A. Hudecova, and engineers T. Honza and E. McFadden. The GLP experiments performed on the NPs were organised by the section leader at the Health effect laboratory, senior scientist E. R. Pran. The transport test of the particles through sandstone was designed by Prof. Dr. O. Torsæter, Dr. A. Delic and M. Omran and conducted by M. Omran. Dr. A. Delic and Prof. Dr. M–A. Einarsrud prepared the manuscript draft. All authors approved the final manuscript. The Research Council of Norway (grant no. 254995), ConocoPhillips, Wintershall Dea, Lundin, Neptune Energy, RES-MAN, and Saudi Aramco have funded this work through the Intelligent Environmental Reporters (INTER) project, a Knowledge-Building Project for Industry.

Conflict of Interests

The authors declare no conflict of interest.

Data Availability Statement

The data that support the findings of this study are available in the supplementary material of this article.

Keywords: Tracer · Luminescence · Nanoparticles · Stöber · Silica

[1] A. Muggeridge, A. Cockin, K. Webb, H. Frampton, I. Collins, T. Moulds, P. Salino, *Philos Trans A Math Phys Eng Sci* **2013**, *372*, 20120320–20120320.
[2] a) V. Alvarado, E. Manrique, *Energies* **2010**, *3*, 1529–1575; b) S. Kokal, A. Abdulaziz, *World Petroleum Council: Official Publication* **2010**, 64–69.
[3] L. Temper, S. Avila, D. D. Bene, J. Gobby, N. Kosoy, P. L. Billon, J. Martinez-Alier, P. Perkins, B. Roy, A. Scheidel, M. Walter, *Environmental Research Letters* **2020**, *15*, 123004.
[4] T. W. Teklu, J. S. Brown, H. Kazemi, R. M. Graves, A. M. AlSumaiti, in *SPE Production and Operations Symposium*, Society of Petroleum Engineers, Oklahoma City, Oklahoma, USA, **2013**, p. 16.
[5] a) D. Tayyib, A. Al-Qasim, S. Kokal, O. Huseby, in *SPE Kuwait Oil & Gas Show and Conference*, Society of Petroleum Engineers, Mishref, Kuwait, **2019**; p. 21; b) Y. Du, L. Guan, in *SPE Asia Pacific Oil and Gas Conference and Exhibition, Vol. All Days*, **2005**; c) H. A. Deans, in *SPE Symposium on Improved Methods of Oil Recovery, Vol. All Days*, **1978**.
[6] S. O. Viig, H. Juilla, P. Renouf, R. Kleven, B. Krognes, Ø. Dugstad, O. K. Huseby, in *SPE International Symposium on Oilfield Chemistry, Vol. All Days*, **2013**.
[7] J. B. Krognes, O. S. Viig, Ø. Dugstad, H. Stray, United States, **2013** https://patents.google.com/patent/US20160003040 A1/en#patentCitations. Last visited on 8th of October, 2023.
[8] a) A.-C. Faure, C. Hoffmann, R. Bazzi, F. Goubard, E. Pauthe, C. A. Marquette, L. J. Blum, P. Perriat, S. Roux, O. Tillement, *ACS Nano* **2008**, *2*, 2273–2282; b) C. Louis, R. Bazzi, C. A. Marquette, J.-L. Bridot, S. Roux, G. Ledoux, B. Mercier, L. Blum, P. Perriat, O. Tillement, *Chem. Mater.* **2005**, *17*, 1673–1682.
[9] I. Hemmilä, *J. Alloys Compd.* **1995**, *225*, 480–485.
[10] T. Rasheed, F. Nabeel, *Coord. Chem. Rev.* **2019**, *401*, 213065.
[11] J. R. Lakowicz, 3. ed., Springer US Boston, Maryland, USA, **2006**.
[12] a) Y.-J. Chuang, F. Liu, W. Wang, M. Y. Kanj, M. E. Poitzsch, Z. Pan, *Sci. Rep.* **2016**, *6*, 27993; b) N. Agenet, P. Perriat, T. Brichart, N. Crowther, M. Martini, O. Tillement, in *SPE International Oilfield Nanotechnology Conference and Exhibition*, Society of Petroleum Engineers, Noordwijk, The Netherlands, **2012**, p. 13.
[13] F. Wang, W. B. Tan, Y. Zhang, X. Fan, M. Wang, *Nanotechnology* **2005**, *17*, R1-R13.
[14] A. Huignard, T. Gacoin, J.-P. Boilot, *Chem. Mater.* **2000**, *12*, 1090–1094.
[15] a) S. Ko, C. Huh, *Journal of Petroleum Science and Engineering* **2019**, *172*, 97–114; b) P. Boul, P. Ajayan, *Energy Technol.* **2020**, *8*.
[16] a) M. Y. Kanj, M. H. Rashid, E. P. Giannelis, in *SPE Middle East Oil and Gas Show and Conference, Vol. All Days*, **2011**; b) Z. H. Yamani, M. H. Al-Jabari, S. A. Khan, S. Ali, M. Y. Kanj, D. V. Kosynkin, M. A. Morsy, *J. Mol. Liq.* **2019**, *274*, 447–454.
[17] S. A. Khan, M. H. Al-Jabari, M. Mansha, S. Ali, Z. H. Yamani, *J. Mol. Liq.* **2022**, *360*, 119505.
[18] G. H. Bogush, M. A. Tracy, C. F. Zukoski, *J. Non-Cryst. Solids* **1988**, *104*, 95–106.
[19] a) Y. Wang, W. Qin, J. Zhang, C. Cao, J. Zhang, Y. Jin, X. Ren, P. Zhu, G. Wei, G. Wang, L. Wang, *J. Nanosci. Nanotechnol.* **2008**, *8*, 1218–1220; b) D. Zhao, W. Qin, C. Wu, G. Qin, J. Zhang, S. Lü, *Chem. Phys. Lett.* **2004**, *388*, 400–405.
[20] C. J. Brinker, G. W. Scherer, *Sol-gel science : the physics and chemistry of sol-gel processing*, Academic Press, Boston, USA, **1990**.
[21] R. M. Almeida, T. A. Guiton, C. G. Pantano, *J. Non-Cryst. Solids* **1990**, *121*, 193–197.
[22] C. J. Brinker, G. W. Scherer, in *Sol-gel science : the physics and chemistry of sol-gel processing*, Academic Press, Boston, USA, **1990**.
[23] A. A. McConnell, R. H. Nuttall®, D. M. Stalker, *Talanta* **1978**, *25*, 425–434.
[24] M. Elbanowski, B. Mąkowska, S. Lis, *Monatshefte für Chemie / Chemical Monthly* **1982**, *113*, 907–913.
[25] a) K. Binnemans, *Coord. Chem. Rev.* **2015**, *295*, 1–45; b) S. K. Gupta, P. S. Ghosh, K. Sudarshan, R. Gupta, P. K. Pujari, R. M. Kadam, *Dalton Trans.* **2015**, *44*, 19097–19110; c) L. Bertry, O. Durupthy, P. Aschehoug, B. Viana, C. Chanéac, *Gold Bull.* **2013**, *46*, 349–355.
[26] M. H. V. Werts, R. T. F. Jukes, J. W. Verhoeven, *Phys. Chem. Chem. Phys.* **2002**, *4*, 1542–1548.
[27] P. K. Gallagher, *J. Chem. Phys.* **1964**, *41*, 3061–3069.
[28] a) Y. Haas, G. Stein, *J. Phys. Chem.* **1971**, *75*, 3668–3677; b) R. D. L. Gaspar, P. R. Fortes, I. O. Mazali, F. A. Sigoli, I. M. Raimundo Jr, *ChemistrySelect* **2018**, *3*, 10491–10501; c) J. L. Kropp, M. W. Windsor, *J. Chem. Phys.* **1965**, *42*, 1599–1608.

[29] a) J. M. Berlin, J. Yu, W. Lu, E. E. Walsh, L. Zhang, P. Zhang, W. Chen, A. T. Kan, M. S. Wong, M. B. Tomson, J. M. Tour, *Energy Environ. Sci.* **2011**, *4*, 505–509; b) M. Omran, S. Akarri, A. Bila, O. Torsæter, in *SPE Norway Subsurface Conference, Vol. Day 2 Tue, November 03, 2020*, **2020**.
[30] T. Hassenkam, C. S. Pedersen, K. Dalby, T. Austad, S. L. S. Stipp, *Colloids Surf. A* **2011**, *390*, 179–188.
[31] M. J. A. de Dood, B. Berkhout, C. M. van Kats, A. Polman, A. van Blaaderen, *Chem. Mater.* **2002**, *14*, 2849–2853.
[32] a) A. Parma, I. Freris, P. Riello, F. Enrichi, D. Cristofori, A. Benedetti, *J. Lumin.* **2010**, *130*, 2429–2436; b) F. Enrichi, *Ann. N. Y. Acad. Sci.* **2008**, *1130*, 262–266.
[33] A. Van Blaaderen, A. Vrij, *Langmuir* **1992**, *8*, 2921–2931.
[34] S. Santra, B. Liesenfeld, C. Bertolino, D. Dutta, Z. Cao, W. Tan, B. M. Moudgil, R. A. Mericle, *J. Lumin.* **2006**, *117*, 75–82.
[35] a) M. Montalti, L. Prodi, N. Zaccheroni, G. Battistini, S. Marcuz, F. Mancin, E. Rampazzo, U. Tonellato, *Langmuir* **2006**, *22*, 5877–5881; b) I. D. Johnson, H. C. Kang, R. P. Haugland, *Anal. Biochem.* **1991**, *198*, 228–237; c) C. Reichardt, *Chem. Rev.* **1994**, *94*, 2319–2358.
[36] Z. Wang, X. Hong, S. Zong, C. Tang, Y. Cui, Q. Zheng, *Sci. Rep.* **2015**, *5*, 12602.
[37] a) R. Songolzadeh, J. Moghadasi, *Colloid Polym. Sci.* **2017**, *295*, 145–155; b) S. Al-Anssari, M. Arif, S. Wang, A. Barifcani, S. Iglauer, *J. Colloid Interface Sci.* **2017**, *508*, 222–229.
[38] M. Yazdimamaghani, P. J. Moos, M. A. Dobrovolskaia, H. Ghandehari, *Nanomedicine* **2019**, *16*, 106–125.
[39] J. G. Croissant, K. S. Butler, J. I. Zink, C. J. Brinker, *Nat. Rev. Mater.* **2020**, *5*, 886–909.
[40] A. Abuelsamen, S. Mahmud, N. H. Mohd Kaus, O. F. Farhat, S. M. Mohammad, F. S. R. Al-Suede, A. M. S. Abdul Majid, *Polym. Adv. Technol.* **2011**, 1–11.
[41] W. Stöber, A. Fink, E. Bohn, *J. Colloid Interface Sci.* **1968**, *26*, 62–69.
[42] E. Glimsdal, I. Dragland, M. Carlsson, B. Eliasson, T. B. Melø, M. Lindgren, *J. Phys. Chem. A* **2009**, *113*, 3311–3320.

Manuscript received: October 22, 2023
Accepted manuscript online: January 17, 2024
Version of record online: January 26, 2024